JCTC Journal of Chemical Theory and Computation

Investigation of Salt Bridge Stability in a Generalized Born Solvent Model

Raphaël Geney,[†] Melinda Layten,[§] Roberto Gomperts,[#] Viktor Hornak,[‡] and Carlos Simmerling*[,†,‡,§]

Department of Chemistry, Graduate Program in Molecular and Cellular Biology, and Center for Structural Biology, Stony Brook University, Stony Brook, New York 11794-3400, and Silicon Graphics Inc., Applications Engineering Group, Hudson, Massachusetts 01749

Received July 29, 2005

Abstract: Potentials of mean force (PMFs) of salt bridge formation between oppositely charged amino acid side chains were calculated both in explicit solvent and in a Generalized Born (GB) continuum solvent model to quantify the potential overstabilization of side chain ion pairs in GB relative to explicit solvation. These show that salt bridges are too stable by as much as 3−4 kcal/mol in the GB solvent models that we tested, consistent with previously reported observations of significantly different structural ensembles in GB models and explicit solvent for proteins containing ionizable groups. We thus investigated a simple empirical correction, wherein the intrinsic GB radii of hydrogen atoms bound to charged nitrogen atoms are reduced, effectively increasing the desolvation penalty of the positively charged groups. The thermodynamics of salt bridge formation were considerably improved, as exemplified by the close match of the corrected GB PMF to the reference explicit solvent PMF, and more significantly by our ability to closely reproduce the experimental temperature melting profile of the TC5b Trp-cage miniprotein, which is otherwise highly distorted by prevalent non-native salt bridges when using standard GB parameters.

Introduction

One of the greatest challenges in the application of computation techniques to biological systems is the accurate determination of protein and RNA three-dimensional structures. The native structure of proteins is maintained at the edge of thermodynamic stability, the free energy of unfolding being in the range of a few kcal/mol. A dominant contributor to stability is the hydrophobic effect, but other important stabilizing factors include van der Waals interactions, hydrogen bonds, and electrostatic interactions, notably salt bridges.[1−3] However, with the stability of salt bridges, i.e., the net balance of favorable Coulombic interactions between opposite charges and their costly desolvation as well as the extent of their involvement in native state stabilization remain ambiguous.[4−9] Nevertheless, salt bridges have been linked to the thermal stability of hyperthermophilic proteins.[1,10−15]

Molecular simulations have proven to be valuable tools for probing the various interactions that define the protein native state and characterize possible folding pathways toward it.[16] Recently, continuum solvent simulations[17−22] have become popular alternatives to their more computationally demanding explicit solvent counterparts, as their lack of solvent friction increases conformational transition rates significantly,[23−31] allowing for faster sampling of the configurational space. Furthermore, because continuum solvent models implicitly average over the water and counterion distributions, this averaging does not need to be done by

* Corresponding author phone: (631)632-1336; e-mail: carlos.simmerling@stonybrook.edu.
† Department of Chemistry, Stony Brook University.
‡ Center for Structural Biology, Stony Brook University.
§ Graduate Program in Molecular and Cellular Biology, Stony Brook University.
# Silicon Graphics Inc.

10.1021/ct050183l CCC: $33.50
Published on Web 11/11/2005

the simulation itself which leads to considerable simplification when calculating thermodynamic properties.[32] Last, some macroscopic solvent properties, such as dielectric effects, are difficult to reproduce accurately with explicit solvation.[33] The ability to build these into implicit solvent descriptions may actually give them some advantage for certain kinds of simulations.

Due to its computational efficiency, the Generalized Born (GB) implicit solvent model[34−36] has become a popular choice to accelerate molecular dynamics (MD) simulations and to study large scale conformational transitions. However, this model lacks structural water features and has been reported to yield higher fluctuations than explicit solvent simulations.[37] To some extent, this might be a consequence of the improved conformational sampling, which lets the simulation more quickly find non-native structures that are energetically favored by the particular force field. But it also seems likely that current GB models do not have as good a balance between protein−protein and protein−solvent interactions as do the more widely tested explicit solvent models. More particularly, we[38] and others[39−42] have observed that salt bridges were frequently too stable in the GB implicit water model, causing salt bridged conformations to be oversampled in MD simulations, thus altering the thermodynamics and kinetics of folding for small peptides. A clear illustration was given by Zhou and Berne,[40] who sampled the C-terminal β-hairpin of protein G (GB1) with both a surface-GB (SGB)[43] continuum model and explicit solvent using a replica-exchange molecular dynamics (REMD)[44] protocol. The lowest free energy state with SGB was significantly different from the lowest free energy state in explicit solvent, with incorrect salt bridges formed at the core of the peptide, in place of hydrophobic contacts. Zhou extended this study on GB1 by examining several force field-GB model combinations,[39] with all GB models showing erroneous salt-bridges. Nevertheless, as the MD simulation community envisions characterizing entire folding landscapes and pathways, implicit solvent models such as GB could be beneficial in supplementing the more slowly converging explicit models but should be devoid of structural bias in order to maintain comparable levels of accuracy.

In this study, the Potential of Mean Force (PMF) of salt bridge formation is calculated for two residues in a solvated protein environment. Masunov and Lazaridis[45] performed similar calculations on isolated side-chain pairs in coplanar monodirectional approaches and concluded that CHARMM GB[46] matches the explicit solvent contact minimum energy to within 1 kcal/mol for both the $Arg^+\cdots Glu^-$ and $Lys^+\cdots Glu^-$ pairs. In our case, comparing salt bridge PMFs obtained either in the GB^{HCT} model[47−50] of AMBER or TIP3P explicit water[51] confirms the excessive strength of salt bridges in this GB model and offers a way to assess its parametrization. A simple empirical change in the assignment of dielectric radii for hydrogen atoms of charged protein groups is investigated and shown to significantly improve the GB PMF of our test salt bridge system. This parameter change is further examined on a range of control systems by comparison to explicit solvent and experimental data.

Methods

All calculations were performed using the AMBER suite of programs,[52] versions 7 and 8, with the ff99 force field[53] modified to improve agreement with ab initio relative energies of alanine tetrapeptide conformations (frcmod.mod_phipsi.1).[38,54] The Trp-cage simulations employed an optimized version of this force field, refit to also reproduce ab initio relative energies of the Gly tetrapepide.[55]

Bonds involving hydrogen atoms were constrained using the SHAKE algorithm,[56] and a 2 fs integration time step was adopted. Explicit solvent simulations were performed with the TIP3P water model,[51] widely popular for its computational simplicity and near-experimental bulk permittivity.[33,57−59] The Fab 17/9 (PDB ID:1HIL[60]) H3 loop fragment and the small helical peptides were placed in truncated octahedral boxes with respectively 5 or 6 Å minimum buffer clearance from the solute.

The Particle Mesh Ewald[61−64] (PME) treatment of long-range electrostatics was used with a direct space cutoff of 8 Å in constant pressure simulations at 1 bar. Implicit solvent runs employed the GB^{HCT} model[47,49,50] with modified Bondi radii[65] and no cutoff. Radii reductions in GB^{HCT} were further applied to hydrogen atoms bonded to nitrogens of N2 and N3 AMBER types,[66] as in Arg, Lys, and charged N-terminal groups.

In the PMF calculations, the varied reaction coordinate was the distance between the carboxyl carbon of the acidic side chain (Cγ in Asp, Cδ in Glu) and either Nζ of Lys or Cζ of Arg, the geometric center of the ionized guanido group. In all cases, the backbone atoms were positionally restrained with sufficient force to prevent significant conformational changes (1 kcal/mol·Å^2 force constant for the Fab 17/9 H3 loop, 10 kcal/mol·Å^2 for the test helical peptides). All PMFs were calculated using Umbrella Sampling (US)[67] with the reaction coordinate constrained to a narrow range by application of a harmonic biasing potential $V(r) = k_{umb}(r - r_0)^2$. US windows were centered every 0.5 Å of the coordinate range (3−11.5 Å) and a 1 ns MD run was performed for each. Umbrella potentials with $k_{umb} = 10$ kcal/Å^2 were applied in all windows, to enforce continuous sampling of high-energy regions. The biased frequency distributions were converted to free energies using the WHAM method,[68] as implemented by Roux.[69] Additional windows were placed at 3.25, 3.75, 4.25, 4.75, 5.25, 5.75 Å for TIP3P simulations, to improve sampling of the barrier region. Data from the first 200 ps of each window were discarded.

To extensively explore the conformational space of the TC5b miniprotein (NLYIQWLKDGGPSSGRPPPS) in the GB^{HCT} solvent model, we employed replica-exchange molecular dynamics simulations (REMD[44,70]) as implemented in AMBER 8. TC5b was modeled in its zwitterionic form, with ionizable residues in their expected ionization state at pH = 7, for a total of 304 atoms. The 267−715.7 K temperature range was covered using 16 replicas (267.0, 285.1, 304.5, 325.2, 347.3, 370.9, 396.1, 423.0, 451.8, 482.4, 515.2, 550.2, 587.6, 627.5, 670.2, 715.7 K), resulting in average exchange acceptance probabilities in the 22−32% range. Exchanges were attempted, and replica conformations were recorded every 500 MD steps (1 ps).

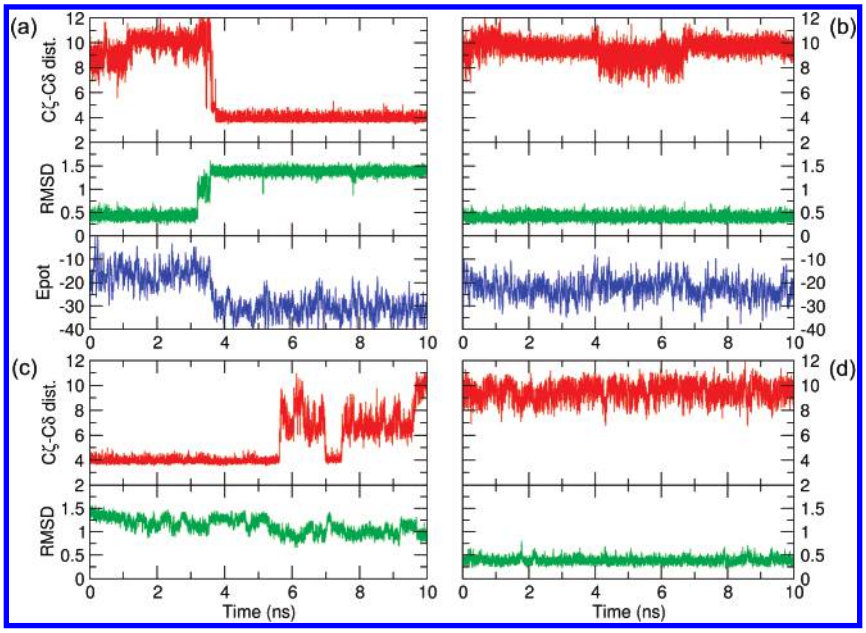

Figure 1. Root-mean-square deviation (RMSD, Å) of Fab 17/9 H3 loop backbone heavy atoms and salt bridge distance (Arg^{97} Cζ−Glu^{100} Cδ, Å) as a function of simulation time, in different conditions at 300 K: (a) GB^{HCT} from native, (b) GB^{HCT} with uncharged Arg^{97} and Glu^{100} side chains from native, (c) TIP3P explicit solvent simulation from salt bridge conformation, and (d) TIP3P from native. The RMSD fit to the X-ray conformation is performed over the restrained, nonloop atoms of the fragment. Relative potential energy values, window averaged over 25 ps, are also reported for implicit solvent simulations in kcal/mol. The backbone transition and concomitant salt bridge formation in GB^{HCT}, not observed with neutralized side chains or explicit solvent, induce a 14 kcal/mol reduction in potential energy.

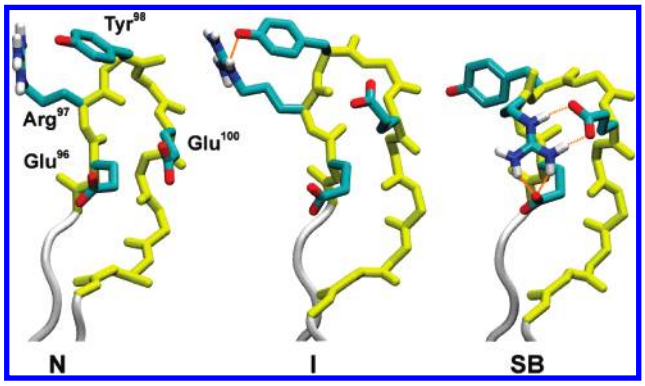

Figure 2. Fab 17/9 H3 loop in native conformation (N), transient intermediate state with inverted Tyr^{98} ψ and Asp^{99} ϕ dihedral angles (I), and stable salt bridged conformation with bidentate H-bond (SB), taken from a standard GB^{HCT} simulation. Loop backbone heavy atoms are colored yellow, while selected side chains are colored by element. H-bonds are indicated by dashed orange lines.

After a 9 ns thermal equilibration period, data were accumulated for 50 ns for each temperature. In GB^{HCT} with standard H^{N+} radii (1.3 Å), the salt bridge strength hampered sampling, and REMD runs were extended to 92 ns in an effort to achieve reasonable convergence.

The Berendsen temperature coupling scheme[71] was applied with a 0.1 ps heat bath coupling constant for all replicas (1 ps for non-REMD simulations). To test the influence of this particular thermostat, the GB^{HCT} PMF profile shown in Figure 4 was recalculated using Langevin dynamics and collision frequency of 1 ps^{-1}. The profile remained essentially unchanged, with a maximum deviation of ∼0.5 kcal/mol from that obtained using Berendsen coupling.

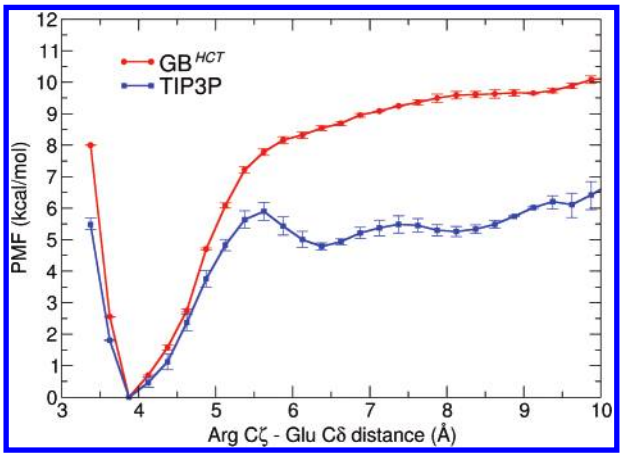

Figure 3. Fab 17/9 antibody Arg^{97}···Glu^{100} ion pair PMF as a function of the intercharged groups distance (Arg^{97} Cζ−Glu^{100} Cδ), at 300 K. The GB^{HCT} PMF overestimates the contact ion pair stability by as much as ∼4 kcal/mol. The loop backbone conformation is restrained in the SB state (Figure 2). Error bars on both curves estimate the sampling error and were derived by separately considering the first or the second half of the data set.

Lower bound estimates of the sampling uncertainty and convergence of our simulation protocols were derived by splitting data sets in half and comparing individual half-length averages to the full-length values.

Results and Discussion

Unstable Behavior of the 17/9 Anti-Influenza Fab H3 Loop in GB Simulations. In the course of our research on loop structure modeling,[72,73] our attention focused on the H3

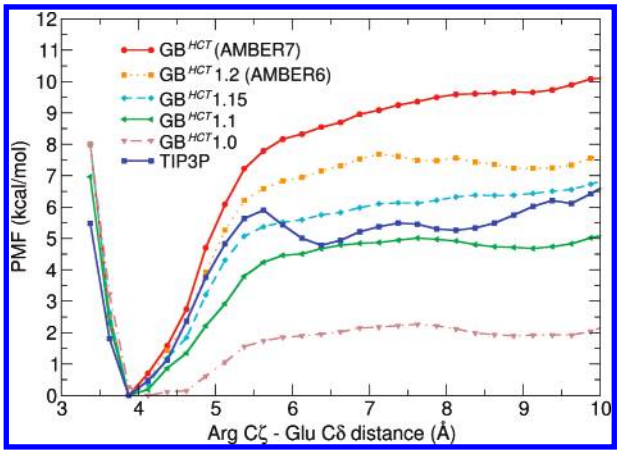

Figure 4. Potentials of mean force for the Fab 17/9 H3 loop Arg^{97}···Glu^{100} ion pair in different solvent models, at 300 K. The distance coordinate is measured between Cζ of Arg^{97} and Cδ of Glu^{100}.

CDR loop of the 17/9 anti-influenza antibody.[60] In preliminary GB^{HCT} MD simulations, its experimentally determined native structure appeared highly unstable, with backbone transitions of nearly 1 Å RMSD magnitude occurring within a few nanoseconds (Figure 1a). This seems unlikely to be attributable to a poorly refined experimental structure, since the 1HIL structure was solved at a reasonable 2.0 Å resolution, and the H3 loop under study is rather well defined, with maximum backbone and side-chain atomic B-factors of 22.08 and 44.82 Å^2, respectively. Nevertheless, this loop incorporates intrinsic flexibility as revealed by crystallography studies that indicate substantial loop rearrangement occurs upon binding to a nonapeptide antigen.[60]

The H3 loop and its surroundings incorporate numerous charged residues, and during simulation, the flexible Arg^{97} side chain (the Kabat antibody sequence numbering convention[74] is followed throughout this paper) associates with Glu^{100}, thereby irreversibly shifting the backbone in a bent non-native conformation (Figure 2). This transformation happens through an intermediate where Tyr^{98} and Asp^{99}, at the tip of the loop, have simultaneously undergone backbone conformational transitions (Figure 2), yet maintaining the hydrogen bond observed between the Arg^{97} and Tyr^{98} side chains in the native state. Rapidly following, the last step of this transformation is the conversion of Arg^{97} from a polyproline II to a left-handed α-helix conformation, simultaneous to salt bridge formation (Figure 2). This last step generates a ~14 kcal/mol drop in potential energy, which effectively locks the loop in the non-native conformation.

Artificially neutralizing both the Arg^{97} and Glu^{100} side chains prevented this behavior (Figure 1b), clearly suggesting the electrostatic nature of the phenomenon, and in particular an imbalance between GB desolvation energy and Coulombic attraction. This control run also evidenced that backbone parameters alone are not responsible for the observed conformational transition.

Even more intriguing was the fact that a TIP3P/PME explicit solvent simulation initiated from the salt-bridged structure saw opening of the Arg^{97}···Glu^{100} ion pair (Figure 1c). However, this was not accompanied by rearrangement of the backbone back to the X-ray conformation during the 10 ns, a process assumed to be slow in explicit solvent. The native loop conformation was also stable throughout a 10 ns TIP3P/PME run started from the X-ray structure, with no salt bridge formation observed (Figure 1d).

PMFs as Measures of GB Deviation from Explicit Solvent Behavior. Owing to the difficulty of directly comparing simulations with experimental salt bridge stability data, mostly of mutational origin, explicit water simulations were chosen as our reference for evaluating the PMF profile of the Fab 17/9 H3 loop Arg^{97}···Glu^{100} salt bridge in GB. As no computationally tractable model—especially not the rigid nonpolarizable model used here—is presently able to correctly reproduce all experimental properties of water,[33] we do not expect to accurately reproduce experimental ion pair behavior. However, the inclusion of solvent molecularity provides a significantly less crude approach than the ad hoc GB model and is used here for consistency with previously published ion pair solvation studies.[45,75−80]

PMFs were obtained in GB^{HCT} and TIP3P explicit solvent using umbrella sampling[67] along the interside-chain distance, with the loop backbone restrained in the SB conformation (Figure 2). The resulting TIP3P profile (Figure 3) consists of a series of well-defined minima: the contact ion pair (CIP) at 3.9 Å, corresponding to the free energy minimum, is accompanied by two solvent-separated ion pair (SSIP) minima at 6.4 Å and 8.2 Å, corresponding to the insertion of one or two TIP3P molecules in the interside-chain volume.[76,81] Qualitatively, the overall shape of the PMF is in good agreement with that reported by Lazaridis for an isolated Arg$^+$···Glu$^-$ pair in a coplanar monodirectional approach.[45] Quantitatively, however, our method yields a barrier height of 6 kcal/mol for going from the CIP to the first SSIP in TIP3P, while the PMF they reported for the isolated Arg$^+$···Glu$^-$ ion pair in the coplanar, double H-bonded approach presents a 7.7 kcal/mol barrier to escape the contact minimum.[45] This slight difference is readily justified by the different solvent exposure levels, approach geometries (cf. Figure 4a,b of ref 45), and presence of a very polar environment around the Fab 17/9 ion pair, with the possibility for Arg^{97} to also interact with Glu^{96}. Gruia et al. similarly calculated the potential of mean force of the Arg^{105}···Glu^{135} salt bridge on the surface of truncated Staphylococcal nuclease (SnaseΔ), after observing in explicit water molecular dynamics simulations that breaking this salt bridge was the rate limiting step of the early unfolding transition.[82,83] Using umbrella sampling, they measured a ~7 kcal/mol transition barrier height for breaking the contact minimum of the two charged side chains.

In contrast to the TIP3P profile, the GB^{HCT} salt bridge PMF shows no depiction of the various SSIPs and grossly overestimates the TIP3P CIP-SSIP energy difference by 3.8 kcal/mol. The activation energy barrier to breaking the salt bridge is also overestimated by almost 2 kcal/mol, providing clear direct evidence for our hypothesis that salt bridges were too stable in this GB model.

The manifestly insufficient desolvation penalty experienced by the salt bridge in GB^{HCT} prompted us to reexamine

the parametrization of this GB solvent model and in particular its handling of cationic protein side chains.

GB Model Parametrization and Rationale for Reduced H^{N+} Radii. The original Born model computes the electrostatic reversible work required to move a charged sphere from a vacuum environment into a continuous high dielectric region. The result is proportional to the square of the charge and inversely proportional to the size of the ion.[84] These ideas were extended to the case of nonspherical solutes in the generalized Born theory,[34,35] which evaluates the electrostatic component of the solvation free energy in the following way:

$$\Delta G_{\mathrm{elec}} = -\frac{1}{2}\sum_i\sum_j \frac{q_i q_j}{f_{\mathrm{GB}}}\left(1 - \frac{1}{\epsilon_{\mathrm{out}}}\right) \quad (1)$$

f_{GB} is designed to interpolate between an effective Born radius α_i at short interatomic distance r_{ij}, and r_{ij} itself at long distances. Various functional forms are possible for f_{GB}, but AMBER employs the analytically differentiable one originally proposed by Still et al.:[35]

$$f_{\mathrm{GB}}(r_{ij},\alpha_i,\alpha_j) = \left[r_{ij}^{\,2} + \alpha_i\alpha_j \exp\left(-\frac{r_{ij}^{\,2}}{4\alpha_i\alpha_j}\right)\right]^{1/2} \quad (2)$$

The effective Born radius α_i corresponds to the radius that would return the electrostatic energy of the system using the original Born equation if all atoms $j \neq i$ in the solute were uncharged. Therefore, α_i reflects the degree of burial of atomic charge q_i from the solute−solvent dielectric boundary. The computation of effective radii in the particular AMBER GB model discussed here (GB^{HCT})[49,50] follows the pairwise descreening approximation (PDA) of Hawkins et al.,[47,48] wherein the molecule is described as a set of atomic spheres of radii ρ_i (eq 3). The corresponding volume integrals can be calculated analytically even when spheres i and j overlap, following eq 13 in ref 47. An additional atom-dependent screening parameter S_i is required in order to avoid overcounting overlap volume between two or more neighboring spheres j, leading to eq 4 which relates all atomic input parameters

$$\alpha_i^{-1} = \rho_i^{-1} - \frac{1}{4\pi}\sum_{j\neq i}\int_{\mathrm{sphere}_j}\frac{1}{r^4}dV \quad (3)$$

with

$$\rho_i = S_i(R_i + b_{\mathrm{offset}}) \quad (4)$$

Although many combinations of S_i, R_i, and b_{offset} could be used, the GB^{HCT} model of AMBER employs screening parameters from the TINKER molecular modeling package[85] and Bondi radii[65] slightly modified for hydrogen atoms, to reflect their bonding environment (Table 1).[49,50] The original b_{offset} value of 0.09 Å, suggested by Still et al.[35] is employed for GB simulations of proteins in AMBER.

Reparametrization of GB^{HCT} for Improved Handling of Ionic Interactions. To correct the stability of the native Fab 17/9 H3 loop conformation, we reasoned that smaller effective GB radii for atoms involved in the salt bridge would increase their desolvation penalty, thus balancing an otherwise dominating Coulombic attraction. Intuitively, formally charged nitrogens can be seen as having increased electronegativity relative to uncharged nitrogens. This should translate in hydrogen atoms bonded to them (H^{N+} atoms) being assigned smaller dielectric radii than H^N atoms, following the suggestion by Tsui and Case that hydrogen GB radii should decrease with increasing electronegativity of their bonding partner.[49] This reasoning is further substantiated by the lower electron density around H atoms in the ammonium ion, relative to ammonia (14% decrease, based on HF/6-31+G* calculations; data not shown). Radii reductions were applied only to hydrogens bonded to nitrogens of N2 and N3 AMBER types,[66] as found in Arg, Lys, and charged N-terminal residues. His protons were not considered, thus far, as their involvement in ionic pairs is less frequent[86,87] and generally weak.[45] Reducing only the radii of H^{N+} atoms also does not greatly affect the overall protein solvation energy (<8% in our tests), while specifically weakening the ion pair. Interestingly, similar ad hoc corrections have been recently proposed by both the Levy and Honig groups, in which additional dielectric screening is applied to oxygen and nitrogen atoms of formally charged groups either through eq 2[42] or eq 4.[88]

Table 1. Parameter Sets Used in the Various AMBER GB Implementations[a]

atom	R_i, GB^{HCT} AMBER6[49]	R_i, GB^{HCT} AMBER7,8[50]	S_i[85]
H^C	**1.3**	**1.3**	0.85
H^N	**1.2**	**1.3**	0.85
H^O	**0.8**	**0.8**	0.85
H^S	**0.8**	**0.8**	0.85
C	1.7	1.7	0.72
N	1.55	1.55	0.79
O	1.5	1.5	0.85
F	1.5	1.5	0.88
P	1.85	1.85	0.86
S	1.8	1.8	0.96

[a] The superscript on H atoms indicates the heavy atom to which it is bound. The H^N R_i value was increased in AMBER7 to stabilize Watson−Crick hydrogen bonds in a 10-base pair DNA duplex.[50]

The GB^{HCT} salt bridge PMF profiles are very sensitive to the choice of H^{N+} radii applied, as a 0.1 Å decrease in radius can produce up to a 3 kcal/mol decrease in stability (Figure 4). Both 1.3 Å and 1.2 Å H^{N+} radii (the standard values in AMBER 7[50] and 6[49] GB^{HCT}) overestimate the TIP3P salt bridge stability by as much as 3.8 and 2.4 kcal/mol, respectively. A 3.8 kcal/mol free energy error by itself is on the same order of magnitude as the folding free energies at room temperature[2] and can have profound consequences on the stability of the ion pair and the structural arrangement of residues around it. In comparison, the 1.1 Å profile adequately captures the energy difference between CIP and SSIP, while the intermediate 1.15 Å H^{N+} radii profile comes close to reproducing the CIP→SSIP barrier height, underestimating it by 0.5 kcal/mol. All GB PMFs lack the solvent-separated minima observed with explicit solvent models, resulting in an absence of barrier to salt bridge formation. This limitation of GB, typical of continuum solvent models,[45] stems from the omission of solvent molecularity and is only

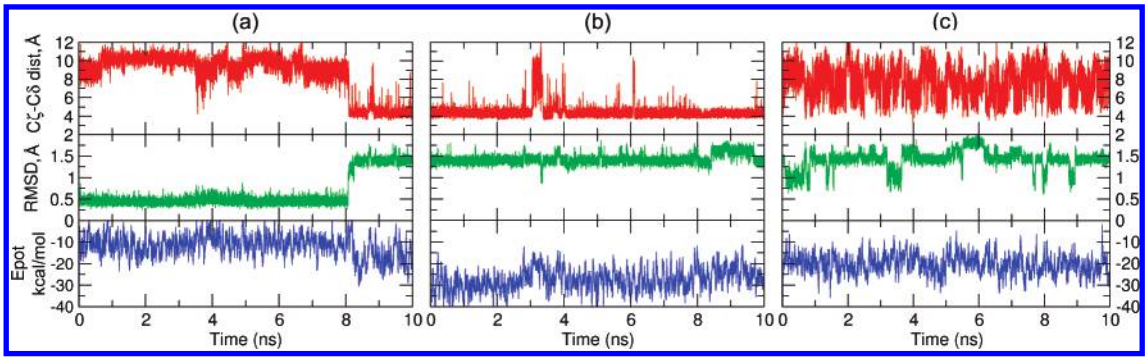

Figure 5. GB^{HCT} simulations of the Fab 17/9 H3 loop with 1.1 Å H^{N+} radii at 300 K, initiated from the X-ray (a) or SB conformations (b). Even with reduced H^{N+} radii, the X-ray loop conformation converts to SB with a 10 kcal/mol decrease in potential energy. The salt bridge, however, reopens transiently in the SB simulation. (c) Simulation from the SB state with neutralized Arg^{97} and Glu^{100} side chains and 1.1 Å H^{N+} radii. Uncharging the salt bridging side chains effectively breaks the salt bridge, but the backbone does not relax back to the native conformation.

addressed in more computationally intensive implicit models such as the RISM formalism,[89−92] molecular surface area-based solvent models,[93,94] or specifically parametrized PB models.[95,96] Employing the recently developed GB^{OBC} model of Onufriev, Bashford, and Case (model II in ref 97) with their suggested Bondi radii[65] modified only for H^N atoms (1.3 Å instead of 1.2 Å) also produced an improved salt bridge profile relative to standard GB^{HCT}, with the PMF underestimating the CIP→SSIP barrier height by 0.5 kcal/mol and overestimating the stabilities of the SSIPs by 0.8 kcal/mol (data not shown, PMF nearly identical to GB^{HCT} H^{N+} = 1.15 Å in Figure 4). As it seems impossible for a simple PDA-based GB model with no depiction of solvent discreteness to capture both the barrier height and the CIP-SSIP energy difference, it seems reasonable to think that GB models should prioritize the correct reproduction of the CIP-SSIP energy gap over the barrier height, since in the absence of solvent discreteness, salt bridge formation is a barrierless downhill process and accurate kinetic behavior cannot be reproduced.

Dynamics were run on the Fab 17/9 H3 loop with H^{N+} radii set to 1.1 Å (Figure 5a), and while the native state could be maintained for an extended period of time (>8ns), the N→SB conversion observed in standard GB^{HCT} still occurs. Because of computational limitations, we could not run a significantly longer or several independent simulations on this system, which would be necessary to fully characterize its kinetic behavior. Yet, a simulation initiated from the SB conformation showed repeated openings of the ion pair, but those events were too transient (<0.5 ns) to allow the loop backbone to relax back to the native conformation (Figure 5c). In contrast, simulations of the SB conformation conducted with the standard radii showed no reopening of the salt bridge (data not shown). Also encouraging was the reduced 10 kcal/mol energy drop accompanying the N→SB transition, down from 14 kcal/mol in standard GB^{HCT} (Figure 1a). This energy difference matches the 4−5 kcal/mol free energy correction visible in the GB^{HCT} 1.1 salt bridge PMF, relative to standard GB^{HCT}, and suggests that additional factors are also responsible for the excessive stability of Fab 17/9 H3 loop non-native conformations. In the following, we take a more systematic approach that is less reliant on backbone parametrization in order to characterize the influence of H^{N+} GB radii on native state stability.

Validation of Radii Modifications on Test Peptides. To assess the relevance of our radii reduction to other systems, including lysine side chains, we studied the PMFs of side-chain ion pairs in small Ala-rich hexapeptides restrained in α-helical conformations. Oppositely charged side chains were spaced one α-helix turn apart (*i*,*i*+4) to create favorable salt-bridge orientations (Figure 6).[98,99] For these simple systems, a stronger positional restraint (10 kcal/mol force constant) was necessary to maintain the backbone in a fully helical conformation.

These exposed salt bridges (Figure 6) displayed markedly reduced stabilities, compared to the Fab 17/9 H3 loop ion pair, due to the absence of a second interacting anionic side chain and the large conformational entropy of the opened state.[100] In particular, the (*i*+4) E,R ion pair, directly comparable to the Fab 17/9 H3 loop ion pair, shows only a 1.2 kcal/mol barrier in TIP3P explicit solvent. This is accompanied by a ∼4 kcal/mol decrease in the CIP-SSIP relative stability from the corresponding pair in Fab 17/9. The same qualitative trend is followed by the GB PMFs, with standard GB^{HCT} still overestimating the stability of the CIP by 2−2.5 kcal/mol, while GB^{HCT} 1.1 falls in close agreement with the TIP3P profile. This improvement suggests that the H^{N+} radii reduction empirically parametrized on the Fab 17/9 salt bridge can be advantageously transferred to other Arg$^+$···Glu$^-$ ion pair geometries.

As observed by Masunov and Lazaridis,[45] the Lys$^+$···Glu$^-$ PMFs tend to be less pronounced, with GB PMFs following, if not accentuating this trend. The discrepancy in interaction energy between GB^{HCT} and TIP3P only fluctuates between 0.7 and 1.6 kcal/mol here, while GB^{HCT} 1.1 falls within 0.5 kcal/mol of the explicit solvent result. This suggests that the GB radii adjustment, while not as crucial as in the stronger Arg$^+$···Glu$^-$ pair, still has the potential to improve the energetics of the Lys$^+$···Glu$^-$ pair appreciably.

Thermodynamical Behavior of the Trp-Cage Miniprotein. As the Fab 17/9 H3 loop native conformation instability appeared to be a coupled salt bridge/backbone problem, we focused our validation effort on Trp-cage TC5b, a miniprotein whose fold has been successfully predicted using long

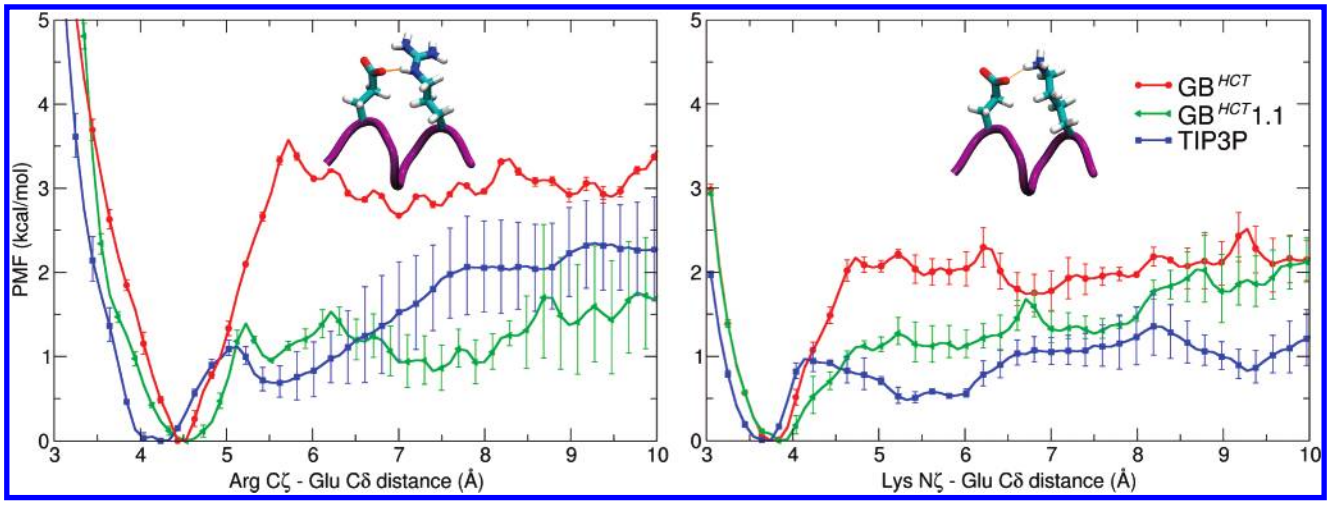

Figure 6. Potentials of mean force of salt bridge formation for the Ac-AEAAARA-NH_2 (left) and Ac-AEAAAKA-NH_2 (right) helical peptides in various solvent models at 300 K. Error bars correspond to separately considering the first or the second half of the data set.

molecular dynamics simulations in implicit solvent,[38] and for which experimental thermodynamic data are available.[101] Even with long MD simulations, there is no assurance that the thermodynamical behavior of protein chains has been sampled to convergence, as some conformational barriers are simply too high to cross on computationally accessible time scales at room temperature. Therefore, we turned to generalized ensemble techniques to evaluate the effect of our GB correction on the thermal stability of charged residue-bearing proteins. However, even generalized ensemble methods such as REMD[44] can require long simulation times to converge, that is why we focused our attention on the TC5b miniprotein construct, a small model (304 atoms), with proteinlike features: a stable fold including tertiary structure and well-defined two state folding kinetics.[101,102] The TC5b construct features an $Arg^{+}\cdots Asp^{-}$ i/i+7 ion pair purposely introduced during the original protein design to generate a stabilizing salt bridge between these positions[101] (Figure 7a). An E5Q mutation was further introduced to avoid forming an unfavorable EXXXD like-charge interaction in the α-helical N-terminal segment of the construct.

Although our lab and others have performed folding simulations of TC5b to near NMR conformations and submitted close to experimental folding rate values,[38,103,104] because of sampling and potential energy accuracy issues, it has proven more challenging to reproduce its full thermodynamic characteristics and in particular experimental melting profiles. The free energy landscape of folding for TC5b has been previously explored by all-atom REMD simulations both in explicit solvent with OPLS-AA[105] by Zhou[106] and implicit solvent using GB^{HCT} and the AMBER ff94[66] force field by Pitera and Swope.[41] Both of these studies predicted significantly higher melting temperatures than the experimental value of 315 K (440 K in TIP3P, ∼400 K in the GB study), raising legitimate doubt about the ability of these force-field/solvation model combinations, parametrized for near-room temperatures, to model temperature-dependent behavior. Additionally, in the implicit solvent study, distorted hydrogen-bonding patterns in solvent-exposed regions of the

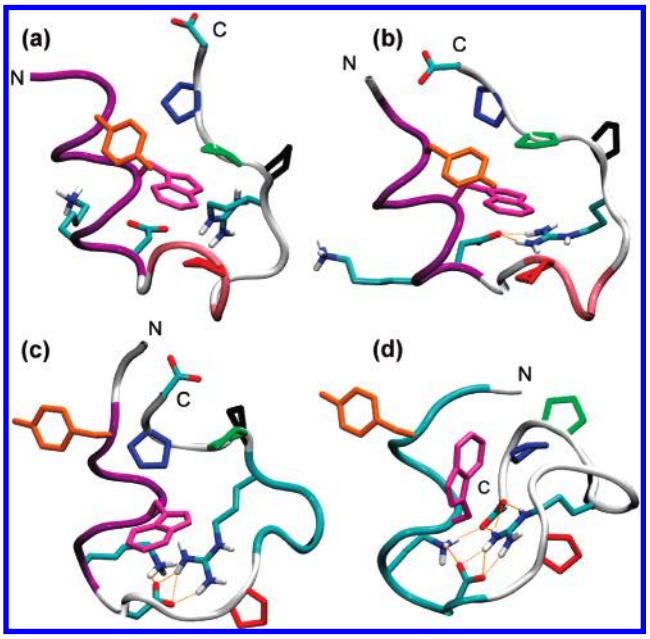

Figure 7. Trp-cage TC5b. (a) Reference NMR structure (model 1 of PDB entry 1L2Y). (b) 267K GB^{HCT} 1.1 REMD global free energy minimum, exhibiting most nativelike features (1.8 Å 3−18 RMSD). (c) 267 K standard GB^{HCT} REMD global minimum and (d) second-lowest free energy minimum, both adopting distorted conformations (2.8 and 3.7 Å 3−18 backbone RMSD, respectively) with multiple salt bridges, not seen in the NMR set. At this temperature in standard GB^{HCT}, the near-NMR ensemble is 1 kcal/mol higher in free energy than the global minimum. The protein backbone is shown in tube representation colored by residue secondary structure type (α: purple, 3_{10}: pink, turn: cyan, coil: white), while Trp-cage motif residue side chains are shown colored as in ref 101: Tyr^{3} (orange), Trp^{6} (magenta), Pro^{12} (red), Pro^{17} (black), Pro^{18} (green), Pro^{19} (blue). Salt bridge forming side chains are colored by atom. H-bonds between ionized side chains are indicated by orange dotted line.

miniprotein were found to cause the largest deviations from the experimental NMR restraints.[41]

Two REMD simulations were performed on the TC5b

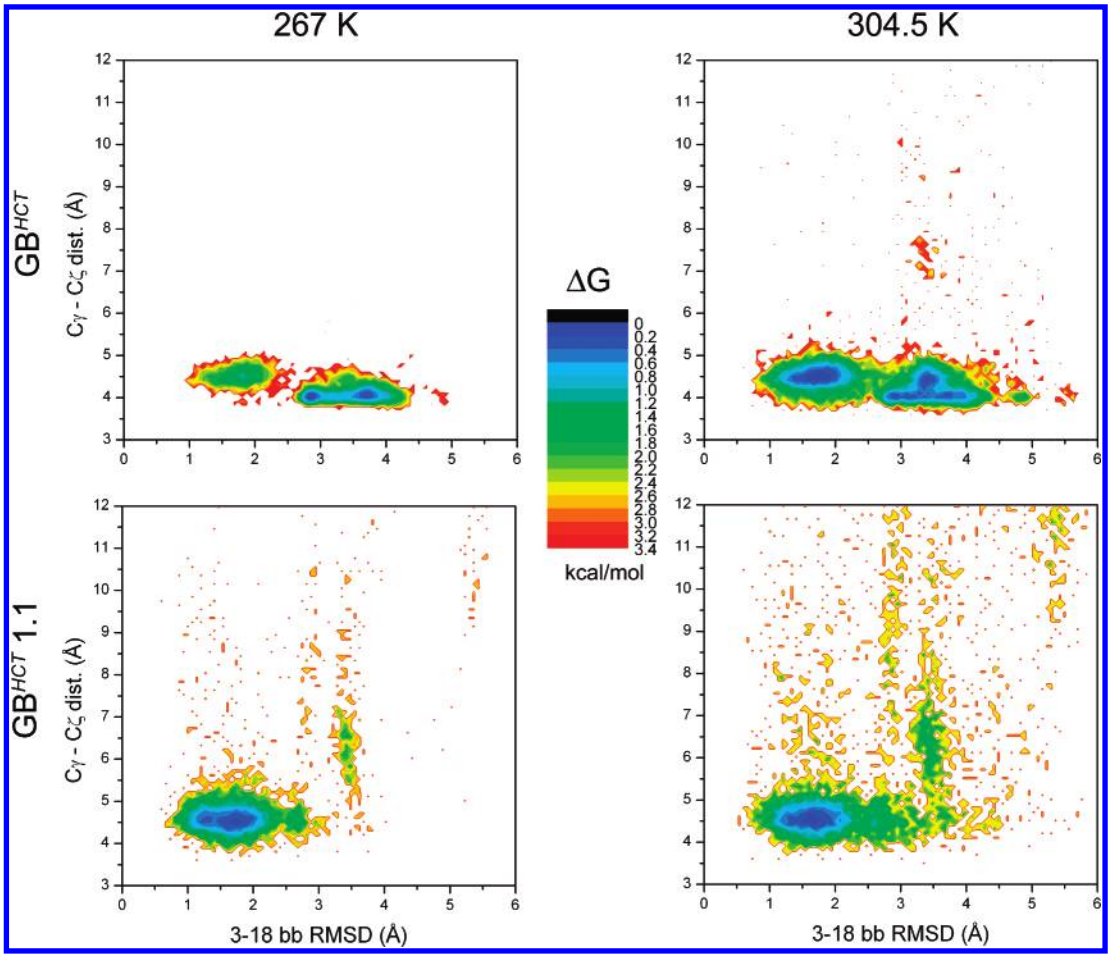

Figure 8. Two-dimensional free energy maps in kcal/mol from REMD data. Top row: GB^{HCT} replicas at 267 K (left) and 304.5 K (right). Bottom row: GB^{HCT} 1.1 replicas at corresponding temperatures. The $Asp^{9}\cdots Arg^{16}$ salt bridge is present in nearly all GB^{HCT} conformations, while it is observed to break more frequently in GB^{HCT} 1.1, particularly for non-native conformations. The average salt bridge distance is *shorter* in the non-native conformations favored by GB^{HCT}. The folded ensemble, which is not the lowest energy basin at 267 K for standard GB^{HCT}, becomes progressively more stable with rising temperature in GB^{HCT}.

construct: one in GB^{HCT} with the standard radii of AMBER8 (modified Bondi[50]), and another with H^{N+} radii set to 1.1 Å, as found optimal for the reproduction of the TIP3P salt bridge PMF in the 17/9 antibody H3 loop study. The simulations covered an extensive temperature range (267−715.7 K) to ensure that high energy barriers did not prevent exhaustive conformational sampling.

Figure 8 shows the TC5b free energy landscapes at various temperatures projected on 2D contour maps using as reaction coordinates the RMSD of backbone heavy atoms in residues 3−18 (corresponding to the well-defined region of the 1L2Y NMR ensemble, with model #1 as reference) and the Asp^{9} Cδ−Arg^{16} Cζ salt bridge distance, to highlight the importance of this ion pair in determining the overall structure of the miniprotein. The lowest free energy basin in standard GB^{HCT} at 267 K (the replica temperature nearest to 0 °C, where experimentally the folded fraction is maximal[101]) comprises only non-native conformations, with a global minimum at 2.8 Å 3−18 RMSD (Figure 7c) and an almost equiprobable ($\Delta G \sim 0.13$ kcal/mol) other minimum at 3.7 Å (Figure 7d). Cluster analysis on the structures comprising this unfolded basin reveals dominant, enthalpically favored ionic networks involving nearly all formally charged moieties of the miniprotein (C-terminal carboxylate, Lys^{8}, Asp^{9}) clustering around Arg^{16} (Figure 7c,d). Once again, these formations underline the insufficient desolvation penalty incurred by charged groups in the standard GB^{HCT} model, as the NMR ensemble shows only one such ionic interaction: the $Asp^{9}\cdots Arg^{16}$ salt bridge. In addition, the Arg^{16} side chain is not well resolved by the NMR assignment,[38] suggesting ample conformational freedom, incompatible with the rigid and thermodynamically stable ionic networks observed in Figure 7c,d.

At 267 K, while the folded region (RMSD < 2.5 Å) is 1 kcal/mol higher in free energy than the global minimum in standard GB^{HCT}, it is the lowest free energy basin in GB^{HCT} 1.1, with a free energy minimum at 1.8 Å RMSD and 4.5 Å salt bridge distance. Structures in this basin still display most of the features of the TC5b native fold: a 2−8 helix (mainly α-helical, according to DSSP[107]) and a second helical segment between residues 11 and 14, with equal proportions of 3_{10}- and α-helical conformations. As a representative structure of the GB^{HCT} 1.1 267 K free energy minimum ensemble shows (Figure 7b), the largest deviation from the NMR reference conformation (Figure 7a) occurs between the 3_{10}-helix and the C-terminal polyproline II segment at Ser^{14} and the flexible Gly^{15}, inducing a slight shift in the location of the polyproline II helix. Nevertheless, the key

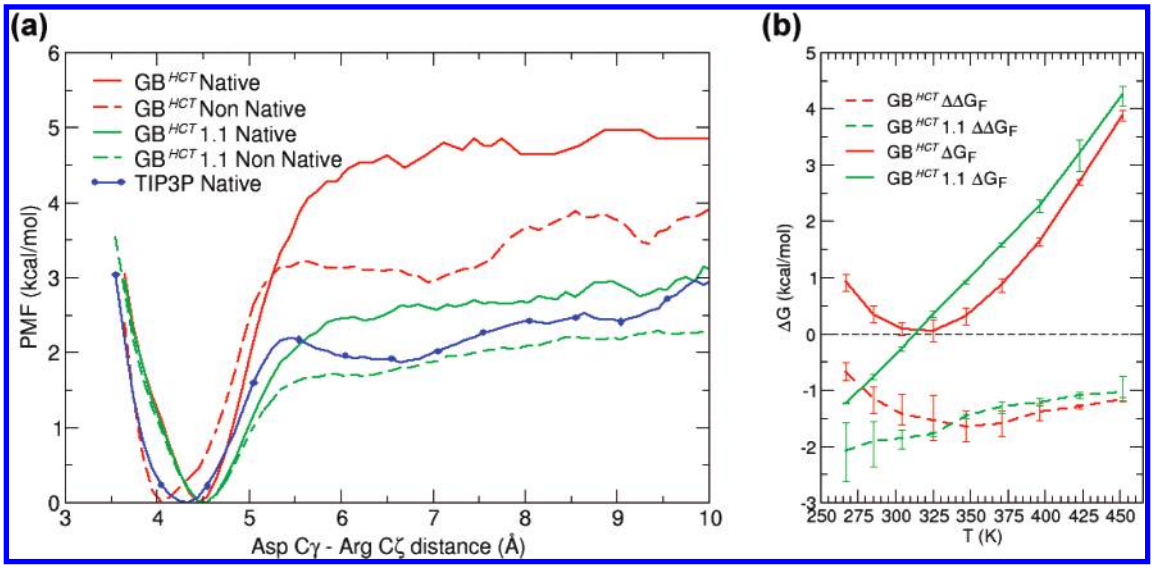

Figure 9. (a) Salt bridge formation PMFs along the Asp[9] Cγ−Arg[16] Cζ distance coordinate for native and non-native ensembles at 304.5 K from REMDs in GB with different radii sets or TIP3P water at 306 K. All curves were smoothed by taking 4-point moving window averages. (b) Native state stabilization by salt bridge, $\Delta\Delta G_F$, as calculated from eq 5 (dashed lines), and folding free energy, ΔG_F (solid lines), in GB^{HCT} with 1.3 Å (red) and 1.1 Å (green) H^{N+} radii. Error bars correspond to separately considering the first or the second half of the data set.

hydrophobic cage motif remains well preserved, with Tyr[3], Trp[6], Pro[12], Pro[18], and Pro[19] clustering nearly as well as in the NMR models. As in the NMR models, the Asp[9]···Arg[16] salt bridge is present, while the Lys[8] side chain is fully solvent exposed and does not take part in intramolecular ionic interactions.

Interestingly, in standard GB^{HCT}, the salt bridge distance distribution is shifted toward longer distances by almost 0.5 Å in the low RMSD ensemble, reflecting the preferential formation of a monodentate H-bond in the near-NMR ensemble ion pair (Figure 7b), while in distorted low free energy structures, a bidentate interaction is favored by the recruitment of Lys[8] in the ionic network (Figure 7c,d). The relative stability of these distorted low-energy structures quickly decreases with temperature, since already at 304.5 K, the properly folded ensemble is more stable by 0.08 kcal/mol. However, the most striking difference between the two GB parameter sets lies in the composition of their respective non-native ensembles.

Salt bridge formation PMFs were calculated at 304.5 K from the GB1.3 and GB1.1 REMD populations and compared to one derived from a short (26 ns) REMD in TIP3P explicit solvent started from the NMR-derived conformation (Figure 9a). This simulation time is sufficient to effectively sample salt bridge distances in the folded state. More details on this explicit solvent REMD simulation will be published elsewhere. The GB^{HCT} 1.1 salt bridge PMF for the native ensemble shows much improved agreement with its TIP3P counterpart, as it marginally overestimates the SSIP stability by ∼0.7 kcal/mol, while standard GB^{HCT} overestimates it by as much as ∼2.7 kcal/mol.

To follow the influence of ion pair strength on the overall stability of the TC5b miniprotein, we calculated the stability contribution of the salt bridge to the folding free energy, $\Delta\Delta G_F$, defined as the difference in free energy of folding of the protein with and without the salt bridge.[108] This quantity corresponds to the free energy difference between forming the salt bridge in the folded and unfolded states:

$$\Delta\Delta G_F = \Delta G_F^{sb} - \Delta G_F^{nosb} = (G_F^{sb} - G_U^{sb}) - (G_F^{nosb} - G_U^{nosb}) = (G_U^{nosb} - G_U^{sb}) - (G_F^{nosb} - G_F^{sb}) \quad (5)$$

Therefore, assuming REMD generates a converged thermodynamic ensemble at each of the replica temperatures, $\Delta\Delta G_F$ was calculated for all REMD temperatures by

$$\Delta\Delta G_F = -RT\ln\left(\frac{p_U^{nosb}\cdot p_F^{sb}}{p_U^{sb}\cdot p_F^{nosb}}\right) \quad (6)$$

where p_U and p_F stand for the unfolded and folded fractions in the absence or presence of the Asp[9]···Arg[16] salt bridge (nosb and sb superscripts, respectively). An RMSD cutoff of 2.5 Å was adopted to define the folded state as it clearly corresponds to the peak of the barrier between native and non-native basins in the 2D PMFs (Figure 8). We defined salt bridged states as having an Asp[9] Cγ−Arg[16] Cζ distance ≤5.5 Å. This value corresponds approximately to the peak of the CIP→SSIP transition barrier in the explicit solvent salt bridge PMF (Figure 9a).

Figure 9b simultaneously shows $\Delta\Delta G_F$ and the overall folding free energy, ΔG_F, for both the standard GB^{HCT} and GB^{HCT} 1.1 REMD simulations. At 304.5 K, the salt bridge stabilization of the folded state is ∼1.4 kcal/mol in GB^{HCT} and ∼1.8 kcal/mol in GB^{HCT} 1.1, well within the range of experimentally observed values.[109]

At low temperatures, the Asp[9]···Arg[16] salt bridge in standard GB^{HCT}, although intrinsically stronger (Figure 9a), actually stabilizes the native state *less* than in GB^{HCT} 1.1. This phenomenon stems from the almost equally strong stabilization of non-native conformations by the salt bridge, as observed in the two compact 267 K GB^{HCT} free energy minima (Figure 7c,d). On the contrary, past 340 K, the salt

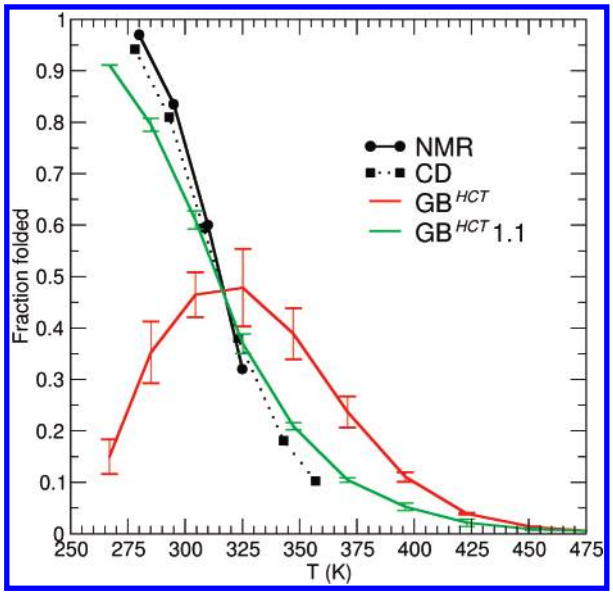

Figure 10. Experimental (CD, NMR CSD)[101] and simulated melting curves for the TC5b miniprotein. Error bars estimating the sampling uncertainty were determined by considering separately the first and second halves of the data set, each 45 ns in GB^{HCT}, and 25 ns in GB^{HCT} 1.1.

bridge contributes more strongly to folded state stability in standard GB^{HCT} than in GB^{HCT} 1.1, at least partly accounting for the increased high-T stability of TC5b in standard GB^{HCT}.

Interestingly, in both GB^{HCT} and the improved GB^{HCT} 1.1 solvent models, salt bridge stabilization decreases much more slowly than the overall protein stability with increasing temperature and remains stabilizing at elevated temperatures, providing a rationale for the increased number of ionic pairs observed in proteins from hyperthermophilic organisms.[1,10,12−15] In addition, the GB^{HCT} model used here, with its constant water dielectric of 78.5, is expected to provide only an underestimation of salt bridge stability at high temperature, as experimentally the dielectric constant of water continuously decreases with temperature, to reach only ∼55 at 100 °C and 1 atm,[110] thus favoring Coulombic interactions even more at high temperatures.[111]

Finally, still using a folding criterion of 3−18 backbone RMSD ≤ 2.5 Å, it is possible to generate melting curves for TC5b in each of the GB models and compare them to experiment (Figure 10). The standard GB^{HCT} produces a melting profile shifted upward by ∼30 K relative to the NMR and CD experimental profiles, as reported by Pitera and Swope.[41] In addition, the preponderance of enthalpically stabilized non-native structures is responsible for the drop in folded fraction at low-temperature seen in the GB^{HCT} profile and even prevents reaching the melting transition midpoint (Figure 10). In sharp contrast, the melting temperature measured by cubic spline interpolation of the melting profile in GB^{HCT} 1.1 (314 K) is in excellent agreement with the experimental value of 315 K.[101] Furthermore, the entire simulated melting profile falls in very good overall agreement with experiment, only departing noticeably (∼10% of fraction folded) from the experimental curves at extremes of the temperature range. We therefore concur with the earlier conclusions by Zhou[106] and Pitera[41] that current force fields are most accurate around room temperature, where they were parametrized. This is especially true of their GB component, which most commonly fails to include the temperature dependence of the dielectric constant. However, current force fields ought to be able to at least predict near-room-temperature melting temperatures, and we show here that in GB^{HCT} this ability was only obscured by the overwhelming influence of incorrectly treated ionic interactions.

Since we did not have to parametrize our potential function against variable temperature data to capture the most important features of the melting profile and a correct T_m value, we believe that the large overapproximations of T_m by earlier REMD studies[41,106] might originate from insufficient sampling caused by overwhelming salt bridges in GB—as was the case in our GB^{HCT} run with standard H^{N+} radii—or solvent friction in TIP3P, preventing reaching ergodicity in either case. In the Pitera and Swope study, the mostly helical TC5b native structure might also have drawn stability from the helical bias of the AMBER ff94 force field[112] that they employed. Although Pitera and Swope employed an energy function very similar to ours (AMBER ff94/GB^{HCT}), they did not report observing the distorted structures with ionic networks we encountered in GB^{HCT}. Possible reasons for this discrepancy could be the small number of replica exchanges attempted in their protocol (400), hampering the sampling of remote regions of the folding landscape by low-temperature replicas, or the excessive stability of helices in ff94 preventing formation of non-native conformations.

Conclusions

Simple GB models based on the pairwise descreening approximation are a popular choice for molecular simulations as they allow significant computational speedup over more accurate GB implementations or PB equation-based implicit solvent models.[113] It is therefore important to ensure that they can achieve an adequate level of accuracy.

Using potentials of mean force, we were able to quantify the problematic overstabilization of ionic pairs observed in the standard GB^{HCT} implementation of the AMBER package. A simple empirical reduction of the GB radii of H^{N+} atoms from 1.3 to 1.1 Å allows a close reproduction of explicit solvent CIP-SSIP relative energies in both the Fab 17/9 H3 loop Arg^{97}···Glu^{100} ion pair and test model helical peptide systems. We note that this ad hoc modification of a single intrinsic Born radius should be followed by a more complete assessment of the influence of all of the radii on the system thermodynamics. In the absence of solvent discreteness, salt bridge formation also remains a kinetically downhill process, and therefore GB models cannot be expected to accurately reproduce the kinetics of conformational transitions. This shortcoming has started to be addressed,[21,22] notably by explicitly including the first solvation shell around solutes in mixed explicit/implicit solvent models.[114−120]

By comparing experimental thermal denaturation data to REMD simulations of the Trp-cage miniprotein TC5b, we confirmed that charge−charge interactions clearly outweigh the desolvation penalty incurred by ionized side chains upon salt bridge formation in the standard GB^{HCT} model of

AMBER. In sharp contrast, the same GB model with only reduced H^{N+} Born radii closely captures the thermodynamics of the $Asp^{9}\cdots Arg^{16}$ salt bridge and for the first time allowed the generation of a near-experimental melting profile for TC5b. The GB^{HCT} 1.1 T_m value of 314 K falls in remarkable agreement with the experimental value of 315 K, while the standard GB^{HCT} profile approaches the melting transition midpoint but shows a disturbing preference for non-native structures at low temperature. While the GB model should at least be capable of correctly predicting thermodynamic observables at or around room temperature, we believe that our accurate reproduction of the TC5b melting profile likely arises from fortuitous cancellation of error, as GB^{HCT} was not parametrized to reproduce the temperature dependence of water solvation.

This study also provides further indication that strong electrostatic interactions are not predominant factors in protein native state stability, as they can stabilize non-native states by similar or even greater amounts, depending on the unfolded state topology.[9,109] Nevertheless, from our modified GB REMD simulation of the TC5b miniprotein, it appears that native state stabilization by ionic interactions decreases at a slower rate than the overall protein stability with increasing temperature, providing a rationale for the observed preponderance of charged amino acid residues in the proteins of thermophilic organisms.[1,10,12−15]

Acknowledgment. Supercomputer time on the NCSA Platinum and Tungsten Linux Clusters (NCSA MCA02N028) and financial support from the National Institutes of Health (NIH GM6167803) are gratefully acknowledged. Additional computer time on a large Altix was generously provided by the SGI Engineering group. C.S. is a Cottrell Scholar of Research Corporation. R. Geney is grateful to the Chemical Computing Group and ACS COMP division for a CCG Excellence Award. The authors also thank Alan Grossfield for making his WHAM code available and David Case, Alexey Onufriev, and John Mongan for helpful discussions.

Supporting Information Available: Full citation for ref 52. This material is available free of charge via the Internet at http://pubs.acs.org.

References

(1) Perutz, M. F. *Science* **1978**, *201*, 1187−1191.

(2) Dill, K. A. *Biochemistry* **1990**, *29*, 7133−7155.

(3) Honig, B.; Yang, A. S. *Adv. Protein Chem.* **1995**, *46*, 27−58.

(4) Honig, B.; Hubbell, W. L. *Proc. Natl. Acad. Sci. U.S.A.* **1984**, *81*, 5412−5416.

(5) Daopin, S.; Soderlind, E.; Baase, W. A.; Wozniak, J. A.; Sauer, U.; Matthews, B. W. *J. Mol. Biol.* **1991**, *221*, 873−887.

(6) Hendsch, Z. S.; Tidor, B. *Protein Sci.* **1994**, *3*, 211−226.

(7) Waldburger, C. D.; Schildbach, J. F.; Sauer, R. T. *Nat. Struct. Biol.* **1995**, *2*, 122−128.

(8) Waldburger, C. D.; Jonsson, T.; Sauer, R. T. *Proc. Natl. Acad. Sci. U.S.A.* **1996**, *93*, 2629−2634.

(9) Dong, F.; Zhou, H. X. *Biophys. J.* **2002**, *83*, 1341−1347.

(10) Elcock, A. H. *J. Mol. Biol.* **1998**, *284*, 489−502.

(11) Xiao, L.; Honig, B. *J. Mol. Biol.* **1999**, *289*, 1435−1444.

(12) Vieille, C.; Zeikus, G. J. *Microbiol. Mol. Biol. Rev.* **2001**, *65*, 1−43.

(13) Zhou, H. X. *Biophys. J.* **2002**, *83*, 3126−3133.

(14) Dominy, B. N.; Minoux, H.; Brooks, C. L. *Proteins* **2004**, *57*, 128−141.

(15) Thomas, A. S.; Elcock, A. H. *J. Am. Chem. Soc.* **2004**, *126*, 2208−2214.

(16) Karplus, M.; McCammon, J. A. *Nat. Struct. Biol.* **2002**, *9*, 646−652.

(17) Cramer, C. J.; Truhlar, D. G. *Chem. Rev.* **1999**, *99*, 2161−2200.

(18) Roux, B.; Simonson, T. *Biophys. Chem.* **1999**, *78*, 1−20.

(19) Simonson, T. *Curr. Opin. Struct. Biol.* **2001**, *11*, 243−252.

(20) Simonson, T. *Rep. Prog. Phys.* **2003**, *66*, 737−787.

(21) Feig, M.; Brooks, I., Charles L *Curr. Opin. Struct. Biol.* **2004**, *14*, 217−224.

(22) Baker, N. A. *Curr. Opin. Struct. Biol.* **2005**, *15*, 137−143.

(23) Kramers, H. A. *Physica* **1940**, *7*, 284−304.

(24) Weiner, J. H.; Pear, M. R. *Macromolecules* **1977**, *10*, 317−325.

(25) Chandler, D. *J. Chem. Phys.* **1978**, *68*, 2959−2970.

(26) Helfand, E. *Physica A* **1983**, *118*, 123−135.

(27) Ansari, A.; Jones, C. M.; Henry, E. R.; Hofrichter, J.; Eaton, W. A. *Science* **1992**, *256*, 1796−1798.

(28) Haran, G.; Haas, E.; Rapaport, D. C. *J. Phys. Chem.* **1994**, *98*, 10294−10302.

(29) Takano, M.; Yamato, T.; Higo, J.; Suyama, A.; Nagayama, K. *J. Am. Chem. Soc.* **1999**, *121*, 605−612.

(30) Karplus, M. *J. Phys. Chem. B* **2000**, *104*, 11−27.

(31) Zagrovic, B.; Pande, V. *J. Comput. Chem.* **2003**, *24*, 1432−1436.

(32) Srinivasan, J.; Cheatham, T. E.; Cieplak, P.; Kollman, P. A.; Case, D. A. *J. Am. Chem. Soc.* **1998**, *120*, 9401−9409.

(33) Guillot, B. *J. Mol. Liq.* **2002**, *101*, 219−260.

(34) Constanciel, R.; Contreras, R. *Theor. Chim. Acta* **1984**, *65*, 1−11.

(35) Still, W. C.; Tempczyk, A.; Hawley, R. C.; Hendrickson, T. *J. Am. Chem. Soc.* **1990**, *112*, 6127−6129.

(36) Qiu, D.; Shenkin, P. S.; Hollinger, F. P.; Still, W. C. *J. Phys. Chem. A* **1997**, *101*, 3005−3014.

(37) Cornell, W.; Abseher, R.; Nilges, M.; Case, D. A. *J. Mol. Graph.* **2001**, *19*, 136−145.

(38) Simmerling, C.; Strockbine, B.; Roitberg, A. E. *J. Am. Chem. Soc.* **2002**, *124*, 11258−11259.

(39) Zhou, R. H. *Proteins* **2003**, *53*, 148−161.

(40) Zhou, R. H.; Berne, B. J. *Proc. Natl. Acad. Sci. U.S.A.* **2002**, *99*, 12777−12782.

(41) Pitera, J. W.; Swope, W. *Proc. Natl. Acad. Sci. U.S.A.* **2003**, *100*, 7587−7592.

(42) Felts, A. K.; Harano, Y.; Gallicchio, E.; Levy, R. M. *Proteins* **2004**, *56*, 310−321.

(43) Ghosh, A.; Rapp, C. S.; Friesner, R. A. *J. Phys. Chem. B* **1998**, *102*, 10983−10990.

(44) Sugita, Y.; Okamoto, Y. *Chem. Phys. Lett.* **1999**, *314*, 141−151.

(45) Masunov, A.; Lazaridis, T. *J. Am. Chem. Soc.* **2003**, *125*, 1722−1730.

(46) Dominy, B. N.; Brooks, C. L. *J. Phys. Chem. B* **1999**, *103*, 3765−3773.

(47) Hawkins, G. D.; Cramer, C. J.; Truhlar, D. G. *Chem. Phys. Lett.* **1995**, *246*, 122−129.

(48) Hawkins, G. D.; Cramer, C. J.; Truhlar, D. G. *J. Phys. Chem.* **1996**, *100*, 19824−19839.

(49) Tsui, V.; Case, D. A. *J. Am. Chem. Soc.* **2000**, *122*, 2489−2498.

(50) Tsui, V.; Case, D. A. *Biopolymers* **2001**, *56*, 275−291.

(51) Jorgensen, W. L.; Chandrasekhar, J.; Madura, J. D.; Impey, R. W.; Klein, M. L. *J. Chem. Phys.* **1983**, *79*, 926−935.

(52) Case, D. A. et al. AMBER 8, University of California, San Francisco, 2004.

(53) Wang, J. M.; Cieplak, P.; Kollman, P. A. *J. Comput. Chem.* **2000**, *21*, 1049−1074.

(54) Beachy, M. D.; Chasman, D.; Murphy, R. B.; Halgren, T. A.; Friesner, R. A. *J. Am. Chem. Soc.* **1997**, *119*, 5908−5920.

(55) Hornak, V.; Roitberg, A. E.; Simmerling, C. Manuscript in preparation.

(56) Ryckaert, J. P.; Ciccotti, G.; Berendsen, H. J. C. *J. Comput. Phys.* **1977**, *23*, 327−341.

(57) Essex, J. W. *Mol. Simul.* **1998**, *20*, 159−178.

(58) Hochtl, P.; Boresch, S.; Bitomsky, W.; Steinhauser, O. *J. Chem. Phys.* **1998**, *109*, 4927−4937.

(59) Richardi, J.; Fries, P. H.; Millot, C. *J. Mol. Liq.* **2005**, *117*, 3−16.

(60) Rini, J. M.; Schulze-Gahmen, U.; Wilson, I. A. *Science* **1992**, *255*, 959−965.

(61) Darden, T.; York, D.; Pedersen, L. *J. Chem. Phys.* **1993**, *98*, 10089−10092.

(62) Essmann, U.; Perera, L.; Berkowitz, M. L.; Darden, T.; Lee, H.; Pedersen, L. G. *J. Chem. Phys.* **1995**, *103*, 8577−8593.

(63) Crowley, M. F.; Darden, T. A.; Cheatham, T. E.; Deerfield, D. W. *J. Supercomput.* **1997**, *11*, 255−278.

(64) Toukmaji, A.; Sagui, C.; Board, J.; Darden, T. *J. Chem. Phys.* **2000**, *113*, 10913−10927.

(65) Bondi, A. *J. Phys. Chem.* **1964**, *68*, 441−&.

(66) Cornell, W. D.; Cieplak, P.; Bayly, C. I.; Gould, I. R.; Merz, K. M.; Ferguson, D. M.; Spellmeyer, D. C.; Fox, T.; Caldwell, J. W.; Kollman, P. A. *J. Am. Chem. Soc.* **1995**, *117*, 5179−5197.

(67) Torrie, G. M.; Valleau, J. P. *J. Comput. Phys.* **1977**, *23*, 187−199.

(68) Kumar, S.; Bouzida, D.; Swendsen, R. H.; Kollman, P. A.; Rosenberg, J. M. *J. Comput. Chem.* **1992**, *13*, 1011−1021.

(69) Roux, B. *Comput. Phys. Commun.* **1995**, *91*, 275−282.

(70) Hansmann, U. H. E. *Chem. Phys. Lett.* **1997**, *281*, 140−150.

(71) Berendsen, H. J. C.; Postma, J. P. M.; van Gunsteren, W. F.; Dinola, A.; Haak, J. R. *J. Chem. Phys.* **1984**, *81*, 3684−3690.

(72) Hornak, V.; Simmerling, C. *J. Mol. Graph.* **2004**, *22*, 405−413.

(73) Hornak, V.; Simmerling, C. *Proteins* **2003**, *51*, 577−590.

(74) Kabat, E. A.; Wu, T. T.; Perry, H. M.; Gottesman, K. S.; C., F. *Sequences of Proteins of Immunological Interest*; Diane Books Publishing Company: 1991.

(75) Bader, J. S.; Chandler, D. *J. Phys. Chem.* **1992**, *96*, 6423−6427.

(76) Rey, R.; Guardia, E. *J. Phys. Chem.* **1992**, *96*, 4712−4718.

(77) Friedman, R. A.; Mezei, M. *J. Chem. Phys.* **1995**, *102*, 419−426.

(78) Resat, H.; Mezei, M.; McCammon, J. A. *J. Phys. Chem.* **1996**, *100*, 1426−1433.

(79) Martorana, V.; La Fata, L.; Bulone, D.; San Biagio, P. L. *Chem. Phys. Lett.* **2000**, *329*, 221−227.

(80) Rozanska, X.; Chipot, C. *J. Chem. Phys.* **2000**, *112*, 9691−9694.

(81) Belch, A. C.; Berkowitz, M.; McCammon, J. A. *J. Am. Chem. Soc.* **1986**, *108*, 1755−1761.

(82) Gruia, A. D.; Fischer, S.; Smith, J. C. *Proteins* **2003**, *50*, 507−515.

(83) Gruia, A. D.; Fischer, S.; Smith, J. C. *Chem. Phys. Lett.* **2004**, *385*, 337−340.

(84) Born, M. *Z. Phys.* **1920**, *1*, 45−48.

(85) Dudek, M. J.; Ponder, J. W. *J. Comput. Chem.* **1995**, *16*, 791−816.

(86) Barlow, D. J.; Thornton, J. M. *J. Mol. Biol.* **1983**, *168*, 867−885.

(87) Kumar, S.; Nussinov, R. *J. Mol. Biol.* **1999**, *293*, 1241−1255.

(88) Zhu, J.; Alexov, E.; Honig, B. *J. Phys. Chem. B* **2005**, *109*, 3008−3022.

(89) Chandler, D. *Annu. Rev. Phys. Chem.* **1978**, *29*, 441−471.

(90) Hirata, F.; Rossky, P. J. *Chem. Phys. Lett.* **1981**, *83*, 329−334.

(91) Hirata, F.; Rossky, P. J.; Pettitt, B. M. *J. Chem. Phys.* **1983**, *78*, 4133−4144.

(92) Pettitt, B. M.; Rossky, P. J. *J. Chem. Phys.* **1986**, *84*, 5836−5844.

(93) Fukunishi, Y.; Suzuki, M. *J. Phys. Chem.* **1996**, *100*, 5634−5636.

(94) Fukunishi, Y.; Suzuki, M. *J. Comput. Chem.* **1997**, *18*, 1656−1663.

(95) Rashin, A. A. *J. Phys. Chem.* **1989**, *93*, 4664−4669.

(96) Pratt, L. R.; Hummer, G.; Garcia, A. E. *Biophys. Chem.* **1994**, *51*, 147−165.

(97) Onufriev, A.; Bashford, D.; Case, D. A. *Proteins* **2004**, *55*, 383−394.

(98) Marqusee, S.; Baldwin, R. L. *Proc. Natl. Acad. Sci. U.S.A.* **1987**, *84*, 8898−8902.

(99) Perutz, M. F.; Fermi, G. *Proteins* **1988**, *4*, 294−295.

(100) Luo, R.; David, L.; Hung, H.; Devaney, J.; Gilson, M. K. *J. Phys. Chem. B* **1999**, *103*, 727−736.

(101) Neidigh, J. W.; Fesinmeyer, R. M.; Andersen, N. H. *Nat. Struct. Biol.* **2002**, *9*, 425−430.

(102) Qiu, L. L.; Pabit, S. A.; Roitberg, A. E.; Hagen, S. J. *J. Am. Chem. Soc.* **2002**, *124*, 12952−12953.

(103) Snow, C. D.; Zagrovic, B.; Pande, V. S. *J. Am. Chem. Soc.* **2002**, *124*, 14548−14549.

(104) Chowdhury, S.; Lee, M. C.; Xiong, G. M.; Duan, Y. *J. Mol. Biol.* **2003**, *327*, 711−717.

(105) Jorgensen, W. L.; Maxwell, D. S.; Tirado-Rives, J. *J. Am. Chem. Soc.* **1996**, *118*, 11225−11236.

(106) Zhou, R. H. *Proc. Natl. Acad. Sci. U.S.A.* **2003**, *100*, 13280−13285.

(107) Kabsch, W.; Sander, C. *Biopolymers* **1983**, *22*, 2577−2637.

(108) Bosshard, H. R.; Marti, D. N.; Jelesarov, I. *J. Mol. Recognit.* **2004**, *17*, 1−16.

(109) Pace, C. N.; Alston, R. W.; Shaw, K. L. *Protein Sci.* **2000**, *9*, 1395−1398.

(110) Fernandez, D. P.; Goodwin, A. R. H.; Lemmon, E. W.; Sengers, J.; Williams, R. C. *J. Phys. Chem. Ref. Data* **1997**, *26*, 1125−1166.

(111) Elcock, A. H.; McCammon, J. A. *J. Phys. Chem. B* **1997**, *101*, 9624−9634.

(112) Cornell, W. D.; Caldwell, J. W.; Kollman, P. A. *J. Chim. Phys.-Chim. Biol.* **1997**, *94*, 1417−1435.

(113) Feig, M.; Onufriev, A.; Lee, M. S.; Im, W.; Case, D. A.; Brooks, C. L. *J. Comput. Chem.* **2004**, *25*, 265−284.

(114) Beglov, D.; Roux, B. *J. Chem. Phys.* **1994**, *100*, 9050−9063.

(115) Lounnas, V.; Ludemann, S. K.; Wade, R. C. *Biophys. Chem.* **1999**, *78*, 157−182.

(116) Topol, I. A.; Tawa, G. J.; Burt, S. K.; Rashin, A. A. *J. Chem. Phys.* **1999**, *111*, 10998−11014.

(117) Rosenhouse-Dantsker, A.; Osman, R. *Biophys. J.* **2000**, *79*, 66−79.

(118) Lee, M. S.; Salsbury, F. R.; Olson, M. A. *J. Comput. Chem.* **2004**, *25*, 1967−1978.

(119) Kentsis, A.; Mezei, M.; Osman, R. *Biophys. J.* **2003**, *84*, 805−815.

(120) Yu, Z. Y.; Jacobson, M. P.; Josovitz, J.; Rapp, C. S.; Friesner, R. A. *J. Phys. Chem. B* **2004**, *108*, 6643−6654.

CT050183L